

Exchange Bias Effect in $\text{La}_{1-x}\text{Ag}_x\text{MnO}_3$ Nanopowders

M. Mihalik¹, M. Antoňák¹, K. Csach¹, M. Fitta², M. Mihalik jr.¹, M. Vavra^{1,3}, M. Zentková¹

¹Institute of Experimental Physics SAS, Watsonova 47, 040 01 Košice, Slovak Republic

²Institute of Nuclear Physics Polish Academy of Sciences, Radzikowskiego 152, 31-342 Kraków, Poland

³Institute of Chemistry, Faculty of Science, PJ Šafárik University, Moyzesova 11, 040 01 Košice, Slovakia

Abstract. Exchange bias (EB) phenomena were first observed in the $\text{La}_{1-x}\text{Ag}_x\text{MnO}_3$ as prepared and heat treated (300 °C/2 hours) nanopowders ($x = 0.10, 0.15$ and 0.20) which were synthesized by self-combustion glycine-nitrate method. These nanoparticles have an average size of about 25 nm and adopt orthorhombic *Pnma* crystal structure. Cooling in magnetic field $H_{cf} \neq 0$ through the Curie temperature T_C shifts hysteresis loop in horizontal and vertical direction. The values of exchange bias field H_E , coercive field H_c , remnant asymmetry μ_E and coercive magnetization μ_c increase with increasing value of cooling field H_{cf} . In addition the training effect was observed. Basic magnetic properties like the Curie temperature T_C and the saturated magnetization μ_s increase and H_E or μ_E decrease with heat treatment. Heat treatment at 600 °C/2 hours increases the average size of nanoparticles to about 55 nm, crystal structure changes to rhombohedral structure (space group $R\bar{3}c$) and EB effect vanishes.

1 Introduction

The exchange bias (EB) was discovered more than 55 years ago, by Meiklejohn and Bean on Co/CoO core-shell nanoparticles [1], and its characteristic signature is the horizontal shift of the centre of magnetic hysteresis loop from its normal position at $H = 0$ to $H_E \neq 0$ and vertical shift which can be characterised by remnant asymmetry μ_E . EB usually occurs in systems which are composed by an antiferromagnet (AFM) that is in atomic contact with a ferromagnet (FM) after the system is cooled, below the respective Néel and Curie temperatures T_N and T_C , in an external cooling field H_{cf} . EB phenomena were observed in various materials like Laves phases, intermetallic compounds and alloys, binary alloys, Heusler alloys [2] or on layered bulk fluorometallo complex [3] where different aspects of magnetism were focused from the EB effect. The first evidence of the EB effect in mixed-valent manganites having perovskite structure was reported in a spontaneously phase separated system $\text{Pr}_{1/3}\text{Ca}_{2/3}\text{MnO}_3$ [4] which stimulated new interest for study of the EB effect in structurally single-phase compounds. The EB phenomena attributed to the spontaneous phase separation are very often observed in manganites with different perovskite structures. In the case of a fine particle system the surface to volume ratio becomes significantly large compared to the bulk counterpart. In such a case the surface effect dominates over the core

part quite often, leading to a variety of magnetism and core-shell model can provide good interpretation of observed phenomena. Both concepts were frequently used for interpretation of EB effects in the $\text{La}_{1-x}\text{Ca}_x\text{MnO}_3$ [5-10], $\text{Nd}_{0.5}\text{Ca}_{0.5}\text{MnO}_3$ [11] and $\text{Pr}_{0.5}\text{Ca}_{0.5}\text{MnO}_3$ [12] nanoparticles. In our paper we report on EB phenomena which were observed in the $\text{La}_{1-x}\text{Ag}_x\text{MnO}_3$ nanopowders with orthorhombic crystal structure. Recent investigations have revealed that replacing the trivalent ion of La by monovalent ion like Ag results in synthesis of room temperature ferromagnetic ceramics [13] or nanoparticles [14] exhibiting colossal magnetoresistance, magnetocaloric effect and similar properties which are typical for manganites where La was partially substituted by the divalent alkali-earth metals.

2 Experimental

Preparation of $\text{La}_{1-x}\text{Ag}_x\text{MnO}_3$ nanopowders ($x = 0.10, 0.15, 0.20$) followed the glycine-nitrate method, which use glycine as fuel and nitrates as oxidants [15, 16]. Within this procedure, the aqueous solutions of the starting compounds were stirred and heated to dehydrate. Afterwards the solutions became viscous gel which underwent an auto ignition after some time. After short combustion of only few seconds, black porous ashes of $\text{La}_{1-x}\text{Ag}_x\text{MnO}_{3-\delta}$ were formed. Thermal analysis performed by TGDTA analyser Setsys16 on as prepared samples revealed thermal processes at about 270 °C

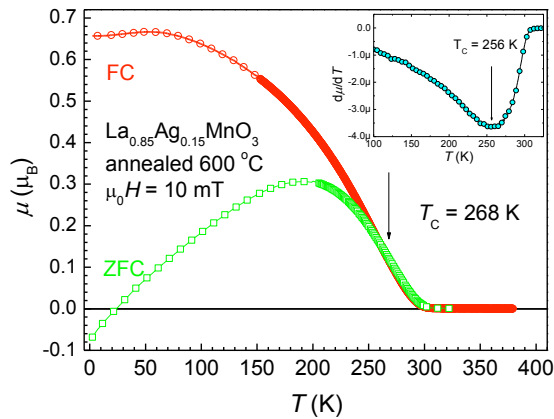


Fig. 1. Temperature dependence of magnetization measured in ZFC and FC regimes. Inset shows our definition of T_C .

which can be attributed to removing of residual material of synthesis. A part of as-cast samples were annealed at 300 °C and 600 °C for 2 hours in air atmosphere by a muffle furnace. The oxygen content (together with mean oxidation state of manganese atoms) in prepared compounds (both as prepared and annealed) was estimated by iodometric titration analysis. The average valence of manganese varies between 3.14 and 3.44 and has a tendency of increasing with x and temperature of annealing. The X-ray powder diffraction (XRD) measurements have been carried out on the X'Pert PRO diffractometer with Cu- K_{α} radiation ($\lambda_1=1.54056 \text{ \AA}$, $\lambda_2=1.54440 \text{ \AA}$) and the XRD patterns were identified with the FullProf program [17] based on the Rietveld method [18]. As prepared and annealed samples at 300 °C crystallize in orthorhombic crystal structure (space group $Pnma$) with lattice parameters close to e.g. $a = 0.56728 \text{ nm}$, $b = 0.77840 \text{ nm}$, $c = 0.55414 \text{ nm}$ ($x = 0.10$, annealed at 300 °C); MnO_6 - building blocks of crystal structure are distorted and tilted. An average size of nanoparticles for both types of samples is about 25 nm. The XRD patterns of both samples contain two additional relatively sharp peaks which cannot be attributed to any relevant

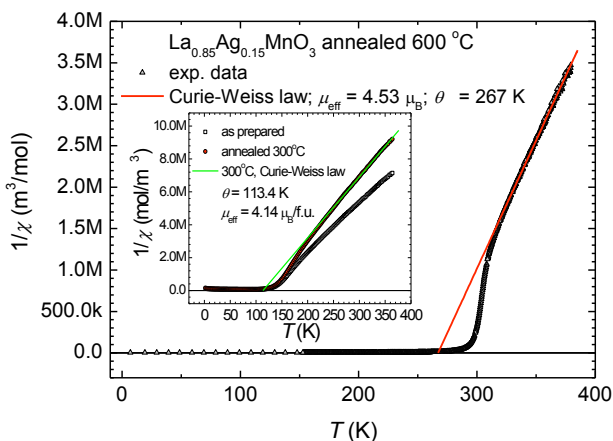


Fig. 2. Inverse susceptibility is shown together with a fit of the Curie-Weiss law for the sample with $x = 0.15$ annealed at 600°C; inset shows $1/\chi(T)$ for as prepared and 300°C annealed samples.

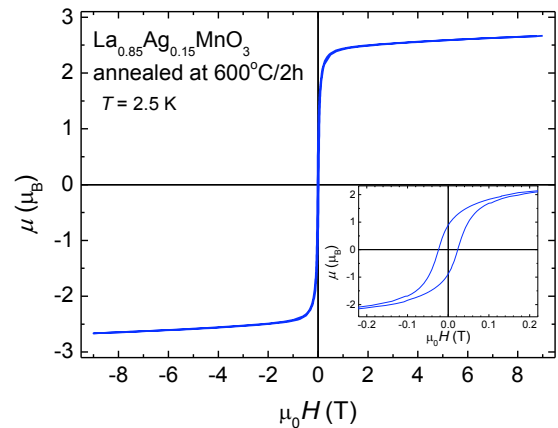


Fig. 3. Hysteresis loop after ZFC cooling; inset shows hysteresis loop in low fields.

nitrate or oxides. Traces of segregated silver were observed on all samples. Silver content increases with increasing temperature of annealing. Samples annealed at 600°C adopt rhombohedral structure (space group $R\bar{3}c$) with lattice parameters close to $a = 0.55035 \text{ nm}$, $c = 1.33540 \text{ nm}$ (sample with $x = 0.1$) and average size of nanoparticles is about 55 nm. Magnetization measurements were realised in the temperature range between 1.8 K and 400 K and in magnetic fields up to 5T or 9 T by a SQUID and VSM magnetometer in MPMS or PPMS, respectively.

3 Results and discussion

Our measurements revealed that all samples undergo a paramagnetic (PM) to ferromagnetic (FM) transition at the Curie temperature T_C . The temperature dependences of magnetization in zero field cooled (ZFC) and field cooled (FC) regimes are shown in Fig.1 for $La_{0.85}Ag_{0.15}MnO_3$ sample annealed at 600°C/2h. The hysteresis behavior between magnetization measurements performed in ZFC and FC regimes for low applied magnetic fields is typical feature of all samples. Bifurcation temperature T_b is comparable with the Curie

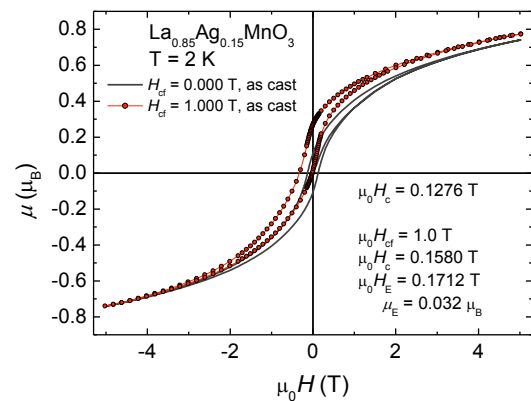


Fig. 4. EB effect is shown for as prepared sample with $x = 0.15$.

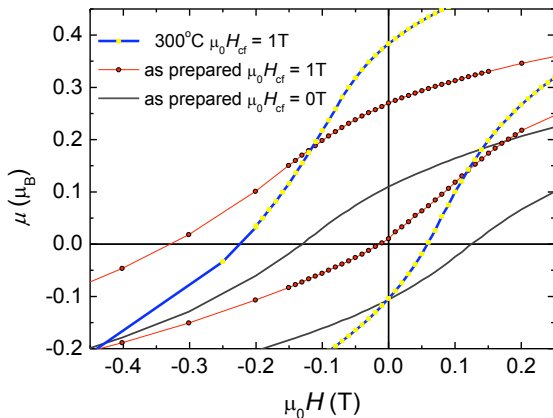


Fig. 5. Sample $x=0.15$. EB effect is weaker on annealed sample; as prepared: $\mu_0 H_E=1647\text{mT}$, $\mu_E=0.1405\mu_B$; annealed at 300°C : $\mu_0 H_E=839\text{mT}$, $\mu_E=0.1385\mu_B$.

temperature T_C and even is a little bit higher for as prepared samples. The Curie temperature was determined as a minimum on $d\mu/dT(T)$ dependence (see inset of Fig.1.). Substitution of Ag for La and subsequent heat treatment increase T_C reaching the maximal value 307 K for sample with $x = 0.2$ annealed at $600^\circ\text{C}/2\text{h}$. Changes of magnetic properties which were induced by increasing of silver content x are much smaller than drastic changes induced by annealing especially performed at 600°C . Heat treatment induces the increase of T_C from 107 K to 121 K and then to 268 K for as prepared, at $300^\circ\text{C}/2\text{h}$ and $600^\circ\text{C}/2\text{h}$ annealed particles of $\text{La}_{0.85}\text{Ag}_{0.15}\text{MnO}_3$, respectively. High temperature magnetic susceptibility χ follows the Curie-Weiss law $\chi = C/(T - \theta)$ for all samples in temperature region high enough above T_C (C is the Curie constant and θ is paramagnetic Curie-Weiss temperature) as it is demonstrated for sample with $x = 0.15$ annealed at $600^\circ\text{C}/2\text{h}$ (Fig.2). The paramagnetic Curie temperature increases with annealing from $\theta = 110$ K to 113 K and finally to 267 K on the sample with $x = 0.15$ and is comparable with T_C . The same tendency we have found on samples with $x = 0.10$ and 0.20 . The increase of T_C and θ with annealing we attribute to oxidation generating higher content of Mn^{4+} in samples which interaction ferromagnetic interaction via double

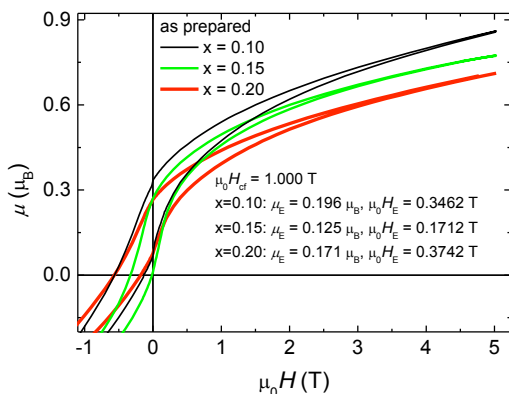


Fig. 6. EB effect is compared on as prepared sample with different chemical composition.

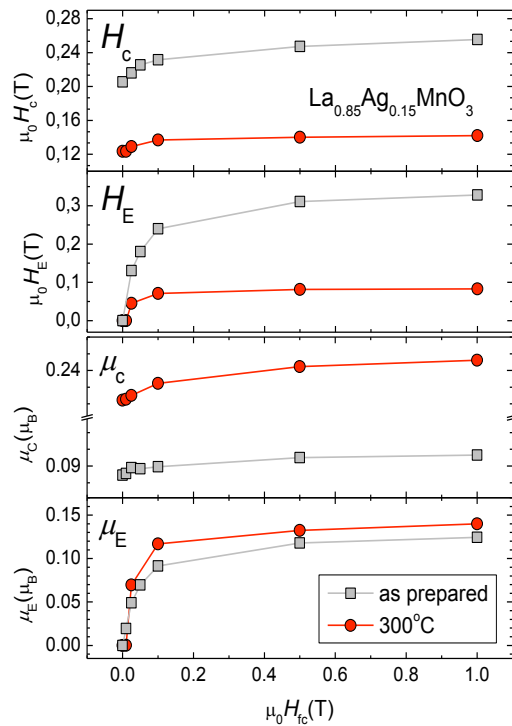


Fig. 7. Summary of EB effect which was measured in fields with induction up to 9 T on sample with $x = 0.15$.

exchange interaction. Evidence for enhanced oxidation was provided by iodometric titration and TG measurements. The effective magnetic moment μ_{eff} changes by non-monotonic way with annealing; at first μ_{eff} decreases from $4.74 \mu_B$ to $4.14 \mu_B$ and then increases to $4.53 \mu_B$ for as prepared, $300^\circ\text{C}/2\text{h}$ and $600^\circ\text{C}/2\text{h}$ annealed samples with $x = 0.15$. The decrease of μ_{eff} can be understood assuming oxidation resulting in higher content of Mn^{4+} in samples and smaller moment can be obtained by the combination of magnetic moments of Mn^{3+} ($4.90 \mu_B$), Mn^{4+} ($3.87 \mu_B$). Annealing at $600^\circ\text{C}/2\text{h}$ will again increase Mn^{4+} content in samples but the effective moment is smaller now. Relation between gradual oxidation and decreasing moment is now not so straightforward and seems to be misleading but the change of crystal structure from $Pnma$ to $R\bar{3}c$ has to be taken into account.

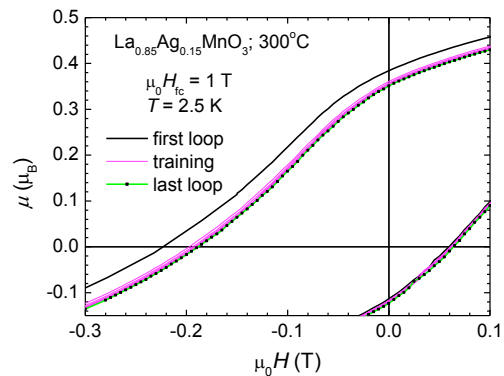


Fig. 8. Training effect was studied on sample with $x = 0.15$.

Two magnetization hysteresis loops which were measured on as prepared sample with $x = 0.15$ are displayed in Fig. 4. First of them was obtained after cooling down in zero magnetic field. Initial magnetization curve starts from zero remnant magnetization and the hysteresis loop is symmetric in respect to zero point of coordinates. Before measurement of second loop the sample was exposed to static magnetic field H_{cf} with induction of 1 T and cooled from 120 K through T_C down to 2K. This procedure gives rise to displacement of the magnetic hysteresis loop, which is the typical manifestation of the EB effect. The loop is pinned on vertex in the region of negative magnetization, is tilt and shifted in horizontal and vertical direction. The horizontal shift of the loop is usually expressed by exchange bias field $H_E = (H_{c+} - H_{c-})/2$ and vertical shift is described by M_E , which is defined as difference of saturated magnetization [2]; H_{c+} and H_{c-} is coercive field on positive and negative axes. In the case that hysteresis loops are not very rectangular another parameter, the remnant asymmetry $\mu_E = (\mu_{r+} - \mu_{r-})/2$, is frequently used [19]; μ_{r+} and μ_{r-} is remnant magnetization on positive or negative axis. The heat treatment at 300°C leads to damping of EB phenomena. Despite of the fact that the coercive magnetization $\mu_c = (\mu_{r+} + \mu_{r-})/2$ increases from 0.130 μ_B to 0.246 μ_B , horizontal shift of hysteresis loop is reduced and vertical shift is nearly unchanged as it can be seen from Fig.5 on sample with $x = 0.15$. EB phenomena were observed on all samples which adopt orthorhombic crystal structure and comparison of EB effect for as prepared samples with different content of x is shown in Fig.6. Saturated magnetization at 5 T decreases with x and horizontal and vertical shift of hysteresis loops is remarkable. All characteristic parameters of EB effect which were obtained in magnetic fields with induction ± 9 T are summarised in Fig.7 which shows effect of cooling field H_{cf} on EB phenomena. All studied parameters have tendency of saturation for relatively low field of about $\mu_0 H_{cf} = 0.1$ T. The heat treatment at 300°C leads to reduction of coercive force H_c and bias field H_E , on the other hand the coercive magnetization μ_c and remnant asymmetry μ_E increase. The difference between subsequent magnetization reversal loops which were measured after cooling in $\mu_0 H_{cf} = 1$ T, the training effect, is shown in Fig.8. Measurement of magnetization reversal loop was repeated 7 times at 2.5 K. Both parameters H_E and μ_E describing the horizontal and vertical shift of loop decrease with consecutive number of cycles and reach stable values.

In conclusion, EB phenomena were observed on ferromagnetic $\text{La}_{1-x}\text{Ag}_x\text{MnO}_3$ nanopowders ($x = 0.10, 0.15$ and 0.20) with average size of about 25 nm which adopt orthorhombic crystal structure (space group $Pnma$). All parameters describing EB effect have tendency of saturation in relatively low field of about $\mu_0 H_{cf} = 0.1$ T. The heat treatment at 300°C leads to reduction of coercive force H_c and bias field H_E , on the other hand the coercive magnetization μ_c and remnant asymmetry μ_E increase. Both parameters H_E and μ_E describing the horizontal and vertical shift of loop decrease with consecutive number of cycles in training effect. Heat treatment at 600 °C/2 hours increases the average size of

nanoparticles to 55 nm, crystal structure changes to rhombohedral structure (space group $R\bar{3}c$) and EB effect vanishes. Our results suggest that surface effects and core shell model can explain EB phenomena in this case because it is well known that surface effect is important on particle with average size smaller than 50 nm. On the other hand magnetic phase separation in single crystalline phase cannot be completely excluded, too.

Acknowledgement: This work was supported by the projects VEGA 2/0057/09, APVV-0132-11, ERDF EU under the contracts No. ITMS26220120005 and ESF EU ITMS626110230034. This work was partially financed by the Foundation for Polish Science.

References

1. W. P. Meiklejohn and C. P. Bean, Phys. Rev.102, 1413 (1956)
2. S. Giri, M. Patra and S Majumdar J. Phys.: Condens. Matter 23, 073201 (2011)
3. Z. Jagličić, M. Zentková, M. Mihalik, Z. Arnold, M. Drofenik, M. Kristl, B. Dojer, M. Kasunič, A. Golobič and M Jagodič, J. Phys.: Condens. Matter 24, 056002 (2012)
4. D. Niebieskikwiat and M.B. Salamon, Phys. Rev. B, 72, 174422 (2005)
5. X. H. Huang, J. F. Ding, G. Q. Zhang, Y. Hou, Y. P. Yao, and X. G. Li, Phys. Rev B. 78, 224408 (2008)
6. S.M. Zhou, S.Y. Zhao, L.F. He, Y.Q. Guo, L. Shi, Mat. Chem. and Phys. 120, 75 (2010)
7. L. Liu, J.J. Zheng, S.L. Yuan, Z.M. Tian, Solid State Communications 150, 1944 (2010)
8. L. Liu, J.J. Zhenga, Z.C. Xia, S.L. Yuan, Z.M. Tian, Solid State Communications 150, 2322 (2010)
9. V. Markovich, I. Fita, A. Wisniewski, D. Mogilyansky, R. Puzniak, L. Titelman, C. Martin, and G. Gorodetsky, Phys. Rev. B 81, 094428 (2010)
10. Xiao H. Huang, Zhen L. Jiang, Xue F. Sun, Xiao G. Li, J. Am. Ceram. Soc., 94, 1324 (2011)
11. L. Liu, S.L. Yuan, Z.M. Tian, X. Liu, J.H. He, P. Li, C.H. Wang, X F Zheng, S Y Yin, J. Phys. D: Appl. Phys. 42, 045003 (2009)
12. T. Zhang and M. Dressel, Phys. Rev. B 80, 014435 (2009)
13. Nguyen The Hien, Nguyen Phu Thuy, Physica B 319, 168 (2002)
14. Manjunath B. Bellakki, C. Shivakumara, N.Y. Vasanthacharya, A.S. Prakash, Materials Research Bulletin 45, 1685 (2010)
15. S. B. Bošković, B. Z. Matovic, M. D. Vlajić, V. D. Krstić., Ceram Int 33, 89 (2007)
16. D. Markovic, V. Kusigerski, M. Tadic, J. Blanus, M. V. Antisari, V. Spasojevic: Scr. Mater. 59, 35 (2008)
17. J. Rodrigues-Carvajal, FullProf.2k Ver. 4.7, ILL., 2010
<http://www.ill.eu/sites/fullprof/php/programs.html>.
18. M.H. Rietveld Journal of Applied Crystallography, 2, (1969)
19. Shilpi Karmakar, S. Taran, Esa Bose, B. K. Chaudhuri, C. P. Sun, C. L. Huang, and H. D. Yang, Phys. Rev. B 77, 144409 (2008)